PROCEEDINGS, 41st Workshop on Geothermal Reservoir Engineering
Stanford University, Stanford, California, February 22-24, 2016
SGP-TR-209

Demonstration of Geothermal Energy Production Using Carbon Dioxide as a Working Fluid at the SECARB Cranfield Site, Cranfield, Mississippi

Barry M. Freifeld[1], Lehua Pan[1], Christine Doughty[1], Steve Zakem[2], Kate Hart[2], Steve Hostler[2]

1. Energy Geosciences Division, Lawrence Berkeley National Laboratory, Berkeley, CA 94720

2. Echogen Power Systems, LLC, Akron, OH 44308

BMFreifeld@lbl.gov

Keywords: Thermosiphon, EGS, CO_2 heat extraction, Cranfield

ABSTRACT

A concept for using supercritical CO_2 ($scCO_2$) to produce geothermal energy was presented by Donald Brown at the Twenty-Fifth Workshop on Geothermal Reservoir Engineering at Stanford University, January 2000. He conjectured that $scCO_2$ would have advantages as a working fluid in comparison to water, with its much greater mobility offsetting the reduced heat capacity and density to provide better heat mining efficiency, along with lower parasitic losses due to $scCO_2$'s large expansivity. In the intervening 15 years there have been numerous theoretical studies suggesting the benefits of using $scCO_2$ as a heat mining fluid, but to our knowledge no field scale demonstration. To test the concept of $scCO_2$ heat extraction, in January 2015 we operated a CO_2 thermosiphon at the SECARB Cranfield Site, Cranfield, Mississippi. The Cranfield Site has been under near continuous CO_2 flood since December 2009 as part of a U.S. Department of Energy demonstration of CO_2 sequestration. Our well pair was perforated at a depth of 3.2 km with a reservoir temperature of approximately 127 °C. The lateral distance between the producer and injector was 100 m, a distance considered pre-commercial in scale, but great enough that thermal breakthrough was still not significant after several years of injection. Instead of producing power with a turbine we extracted heat from our recirculated fluid using a heat exchanger and portable chiller. The wellfield and surface equipment were heavily instrumented to enable a comparison of numerical models with field observations. In the end our thermosiphon did not meet our predicted flow rates or energy production rates. We will explore the reasons why our predictions diverged from our observations in this presentation and make suggestions for future research needed to advance the concept of heat extraction using $scCO_2$.

1. INTRODUCTION

Brown (2000) first proposed using CO_2 in place of water as the working fluid for extracting geothermal heat. However, replacing water with CO_2 is hampered by the lack of widespread naturally occurring CO_2 sources. However, the widespread adoption of geologic carbon sequestration (GCS), where CO_2 from point sources such as power plants, oil refineries, and ethanol processing facilities are captured and stored underground, will drastically increase the availability of CO_2. Coupling GCS with geothermal energy production can offset some of the incremental costs associated with carbon capture, and end up benefitting both industries.

The primary benefits cited for using CO_2 as a replacement for water are: (1) its large compressibility and expansivity, which can lead to creation of a natural thermosiphon, wherein CO_2 circulates without the need for external pumping; (2) lower viscosity; and (3) reduced chemical interaction with rock minerals. While CO_2 has a smaller heat capacity than water, when considered in light of its lower viscosity, the greater mobility leads to a net overall increase in efficiency (Pruess, 2006). Pruess (2006) performed detailed numerical reservoir simulations of a classic five-spot well pattern comparing CO_2 with water, assuming realistic thermophysical parameters. His results show that there is a broad range of pressures and temperatures at which there is a significant benefit in using CO_2. However, Pruess (2006) simplified the physics of heat and fluid flow in the wells, considering them under isenthalpic and gravitationally static conditions, to produce estimated wellhead conditions. This ignores the heat transfer between the wells and the surrounding formation, as well as frictional and inertial forces within the wells. We account for all these features in the models employed in the present work.

The Cranfield Test was designed to explore the potential for using CO_2 as a working fluid for geothermal energy production. It was conducted at the SECARB Cranfield CFU31 site, the location of a previous U.S. Department of Energy project to demonstrate GCS in a saline aquifer, operated by the South Eastern Regional Partnership for Carbon Sequestration (SECARB). The well site consists of three wells: an injector CFU-31F1 (here called F1) and two collinear observation wells, CFU-31F2 (called F2) about 70 m away, and CFU-31F3 (called F3) another 30 m away. All wells are perforated in the highly heterogeneous, highly permeable, brine-saturated Tuscaloosa sand, which is 3.2 km deep, about 23 m thick, and dips downward at 1-2 degrees from F1 toward F3. Ambient pressure is 325 bars and temperature is 129 °C.

In order to analyze the field data from the Cranfield Test, we used a series of three numerical models including the reservoir, the injection and production wells, and the surface equipment. The first model considers a hypothetical commercial-scale reservoir and assumes that CO_2 is the only fluid present. It predicts a sustaining thermosiphon for a range of flow rates and wellbore conditions. The second model is based on the SECARB Cranfield CFU31 site and includes the long-term CO_2 injection that preceded the Cranfield Test to create a two-phase CO_2/brine system. It also predicts a sustaining thermosiphon. These two models were developed before the Cranfield Test was conducted and their positive results were what motivated us to go to the field. The third model is similar to the second model, but was developed after the Cranfield Test and includes a more realistic representation of the surface equipment and the

actual schedule of field activities. It also predicts a sustaining thermosiphon, in contrast to the field data, which show a decaying thermosiphon that cannot be sustained.

The structure of the paper is as follows. First, we show the results of the first two numerical models. Then we describe the field test and data obtained, which are compared to results of the third numerical model. Next we present a series of hypotheses to explain the discrepancies between the models and the field data, specifically why the models predict that a thermosiphon can be sustained whereas the field data show that the thermosiphon decays quickly. We include plans for future work to test these hypotheses.

2. MODEL PREDICTIONS OF CO_2 THERMOSIPHON BEHAVIOR

2.1 Hypothetical Site with Single-Phase scCO_2

We developed a rigorously coupled wellbore-reservoir model of geothermal heat extraction using CO_2 as the working fluid. We consider the classic 5-spot problem presented by Pruess (2006), shown schematically in Figure 1. Since they serve as pathways from surface to reservoir, the injection and production wells play important and unique roles in a geothermal heat extraction system. In our model, the wellbore flow and the reservoir flow are seamlessly coupled together, although they are governed by different physical laws. Therefore, complex interactions between the wellbore processes and the reservoir processes can be investigated.

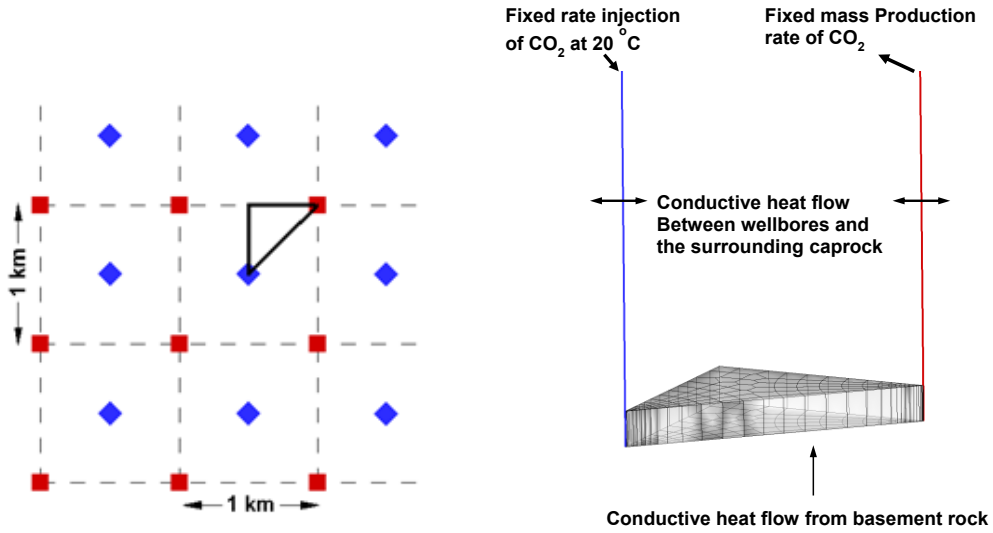

Figure 1. Plan view (left) and perspective view (right) of the 1/8th symmetry element used for the all-CO2 model.

The thermophysical properties of the compressible CO_2 make the coupling between the reservoir and the wellbores stronger and more complicated than when using water as the working fluid. Using a decoupled model would not be able to capture those important interactions and could lead to misleading conclusions. We use a fully coupled wellbore-reservoir simulator, T2Well (Pan et al., 2011a, 2011b, 2011c; Pan and Oldenburg, 2013), which incorporates the widely used reservoir-simulation code TOUGH2 (Pruess et al., 1999), with the TOUGH2 equation of state module ECO2H. ECO2H, as an extension of ECO2N (Pruess and Spycher, 2007), includes a comprehensive description of the thermodynamic and thermophysical properties of a H_2O-NaCl-CO_2 system in the pressure and temperature ranges for typical geothermal systems (up to 67.6 MPa and 243 °C). In T2Well/ECO2H, we treat the wellbore-reservoir flow problem as an integrated system in which the wellbore and reservoir are two different subdomains where flow is controlled by different physics. Specifically, viscous flow in the wellbore is governed by the 1D momentum equation, and 2D flow through the porous reservoir is governed by a multiphase version of Darcy's law. As a result, the governing equations for the flow processes in the wellbore-reservoir system are an extended set of those used by the standard TOUGH2. The major differences in the governing equations between the wellbore and the reservoir are the definitions of energy-flow terms and the phase velocities. Both kinetic energy and gravitational potential energy are included in wellbore energy-balance equations, but they are neglected in reservoir energy-balance equations. Meanwhile, the phase velocities in the reservoir are simply determined by Darcy's law as the Darcy velocity (volume flux), whereas the phase velocities in the wellbores are calculated from the mixture velocity and the drift velocity according to the Drift-Flux-Model (DFM).

The geothermal reservoir we consider here is an idealized 100 m thick porous reservoir with 25% porosity and 100 mD permeability. The pore space of the reservoir is assumed to be initially filled with supercritical CO_2 at hydrostatic pressure (29.15 MPa) and geothermal temperature (152.2 °C) conditions, representing a reservoir at a depth of 3000 m in a relatively high geothermal heat flow region such as the Texas Gulf Coast.

We first simulated two fixed flow rate cases (5 kg/s and 25 kg/s) in which CO_2 (at 25°C) is injected at the injection wellhead at the specified flow rate, while the same amount of CO_2 mass is produced at the production wellhead. The production-wellhead pressure remains much higher than the injection-wellhead pressure after a short kick-off period (Figure 2). This implies that it is possible to establish a thermosiphon mechanism for geothermal heat extraction using CO_2 as the working fluid. Furthermore, the average injection-wellhead pressure for a 25 kg/s flow rate is even lower than that for 5 kg/s flow rate. In other words, it is easier to set up a siphon system

for a higher flow rate than for a lower flow rate. This unique feature is related to the strong dependence of CO_2 density on temperature. In a higher flow-rate injection well, the higher velocity and greater inflow of cold CO_2 makes the lateral heat gain from the surrounding caprock less important, which makes the overall CO_2 temperature lower than it would be in a lower flow-rate injection well. As a result, the CO_2 in a higher flow-rate injection well is colder and denser than in a lower flow-rate injection well, which requires a smaller wellhead pressure to maintain the given well-bottom pressure for driving flow into the reservoir. For a similar reason, the CO_2 in a higher flow-rate production well is warmer and lighter than in the lower flow-rate case, which results in a higher production-wellhead temperature in the higher flow-rate case.

We also studied the effect of varying well diameter, tubing diameter, and heat exchange properties between the wellbore and the overburden on thermosiphon behavior, and considered a range of higher flow rates (Figure 3). When the flow rate goes too high, both the pressure loss due to friction to the well wall and the reservoir pressure drop due to widespread cooling would become dominant and destroy the benefit of smaller lateral heat exchange obtained for the higher flow rate. Thus, we conclude that there is an optimum flow rate in terms of system performance for a given system with certain reservoir conditions and well configurations. More details of this work may be found in Pan et al. (2015b).

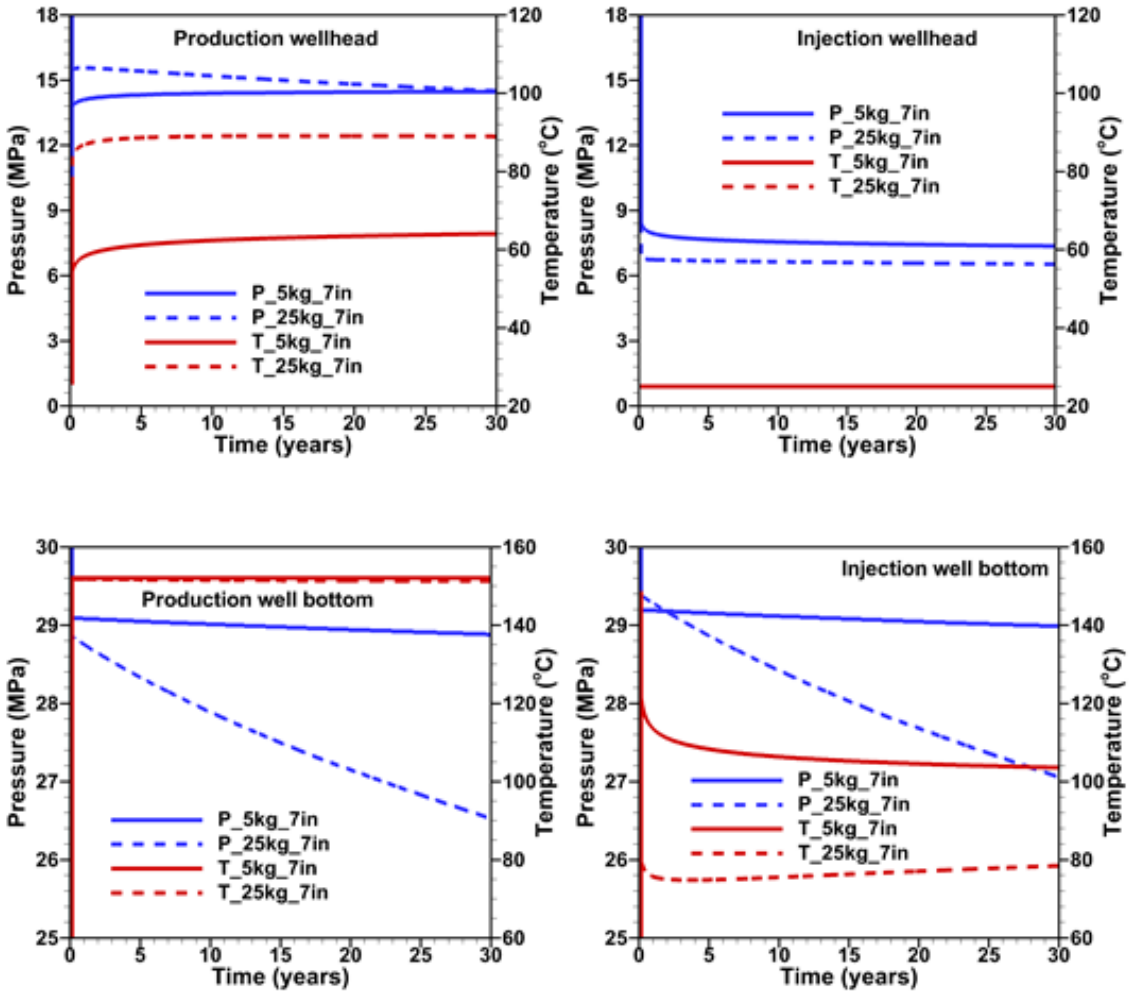

Figure 2. Summary of wellbore pressure and temperatures for the all-CO_2 simulations for two flow rates: 5 kg/s and 25 kg/s. The unique properties of CO_2 enable a pressure gradient from producer to injector at the wellhead and from injector to producer at the reservoir, creating a sustaining thermosiphon.

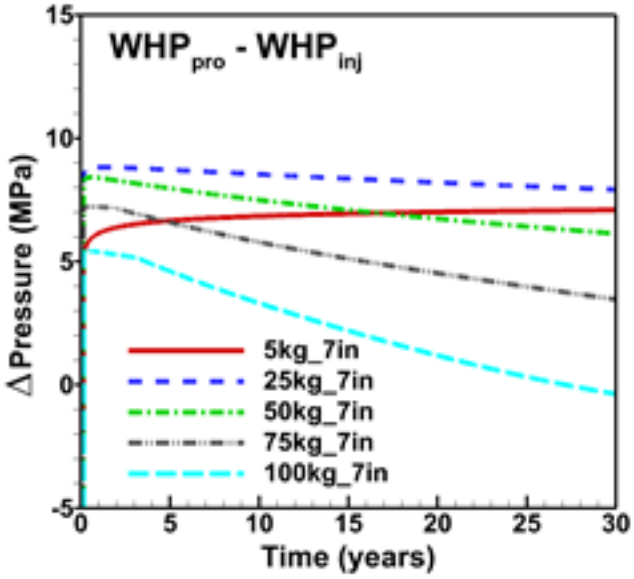

Figure 3. Wellhead pressure difference between producer and injector for high flow rates for the all-CO_2 simulations. Sustaining thermosiphons are possible for a large range of rates.

2.2 Actual Cranfield Conditions with Two-Phase scCO_2 and Brine

We use the same computational capabilities of T2Well described in the previous section, but apply it to a model of the SECARB Cranfield CFU31 site. The reservoir and well portions of the grid is shown in Figure 4, it also includes cells to represent the surface equipment and piping. The simulation period begins in December, 2009 with the onset of CO_2 injection into well F1, which continues until April, 2014, at which time a thermosiphon using production from well F3 and injection into well F1 is initiated. Reservoir parameters are taken from modeling studies used to analyze the GCS operation of the site, which involved model calibration to pressure, temperature, CO_2 breakthrough observations, and geophysical data (Doughty and Freifeld, 2013; Hosseini et al., 2013; Doetsch et al., 2013). The reservoir consists of six layers with porosities and permeabilities taken from F1 well logs (Table 1).

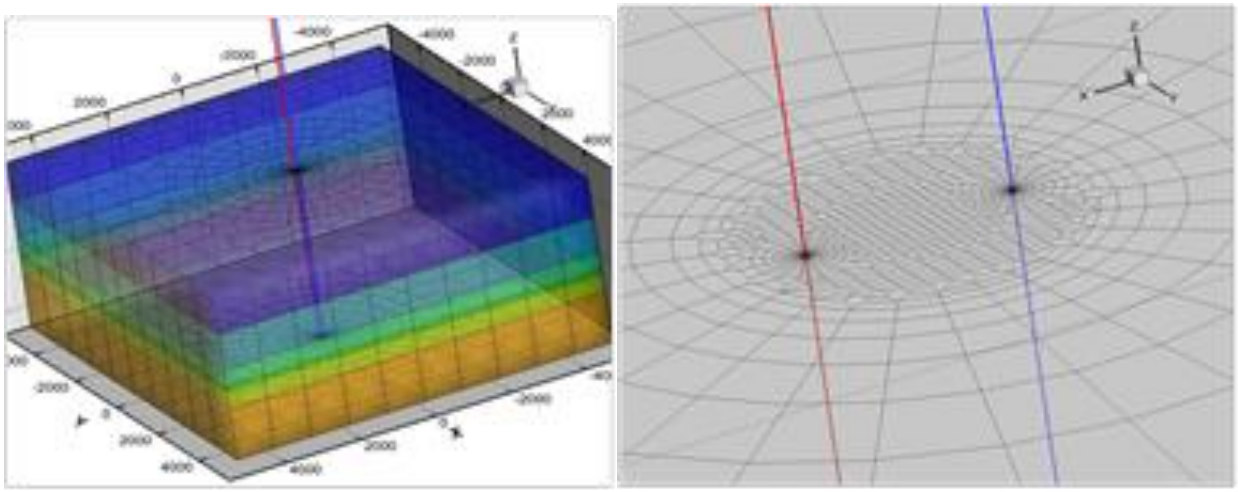

Figure 4. 3D grid of the reservoir with two wells for the Cranfield CFU31 site model. Blue line indicates the injection well and red line indicates the production well. Entire mesh (left) and local refinements (right).

Table 1 Formation layers and their properties for Cranfield CFU31 site models.

Name	Thickness (m)	Porosity	Lateral perm. (mD)	Vertical perm. (mD)
Layer1	6.86	0.169	8.60	1.058
Layer2	6.10	0.254	130.7	1.058
Layer3	2.90	0.288	230.0	47.94
Layer4	0.90	0.139	2.4	0.082
Layer5	3.00	0.315	349.2	84.87
Layer6	3.40	0.283	225.7	2.229
skins	0.1679 (lateral)	0.139	1.35	0.1058

Note that at the onset of thermosiphon modeling, water in the reservoir is all immobile (after many years of flushing with CO_2) and with a low value of $S_{lr} = 0.01$ chosen, there is little water in the reservoir.

Similar to the all-CO_2 model, where fixed injection and production rates were specified at the wellheads, here the flow from F3 to F1 is fixed at a cell representing the flow rate control valve in a section of the surface pipe. The pressure gradient across this cell this then checked, and if pressure on the F3 side of the cell is higher than pressure on the F1 side, a thermosiphon is inferred. We define the siphon force as the difference between the pressure drop across the cell and the pressure drop over the same length of a normal section of the same flowing pipe. For any given mass flow rate, if the siphon force is positive, a thermosiphon is possible, otherwise, a pump is required to maintain the flow rate. The thermosiphon test consists of three step-tests, each a week apart. Each test consists of four mass flow rates sequentially, namely, 2, 4, 6, and 8 kg/s. Each step lasts for 12 hours. Between the three step-tests, the mass flow rate is maintained at a constant value of 5 kg/s. Additional special cells in the surface piping represent a gas/liquid separator (which would be needed if the well effluent were going to a power plant) and a condenser to remove heat from the CO_2 before it is reinjected into well F1 (because there is no actual power plant). To kick-off the thermosiphon, we need to increase the pressure of the production wellhead over that of the injection wellhead. To accomplish this, we assume that the ongoing injection of CO_2 from the outside source is cooled by a condenser, which reduces the injection wellhead pressure.

Simulation results show that the siphon force increases with a decrease of the mass flow rate and vice versa (Figure 5a). As mass flow rate increases to 8 kg/s, the siphon force becomes negative, indicating an additional pump is needed to maintain this flow rate, thus a thermosiphon is not sustainable at this rate for this system. The wellhead pressure responses to the mass flow rate are opposite between the production well and the injection well (Figure 5b). As mass flow rate increases, the production wellhead pressure decreases but the injection wellhead pressure increases. However, the magnitude of this response is larger in the injection well than in the production well. Meanwhile, the production well bottom pressure is much less sensitive to changes in mass flow rate than is the injection well bottom pressure. Similar patterns can be seen in the temperatures responses (Figure 5c). The liquid saturation at various locations changes little except immediately after a switch in mass flow rate (Figure 5d).

Two sensitivity studies were done to investigate the role of liquid mobility. In one case, the wellbores were arbitrarily made drier by increasing the residual liquid saturation for the thermosiphon simulation, without altering the initial saturation distribution in the reservoir. Hence the same amount of liquid water was present in the reservoir, it just could not move up the wellbore. This changed increased the siphon force at all flow rates, and it remained positive even at the highest flow rate. In the other case, a more realistic variation was to choose relative permeability functions in which gas relative permeability was larger and liquid relative permeability was smaller than in the base case, and simulate the initial CO2 injection period, the kick-off stage, and the thermosiphon operation. In this case, changes to the siphon force were smaller, and changed sign depending on the flow rate. More details of this work may be found in Pan et al. (2015a).

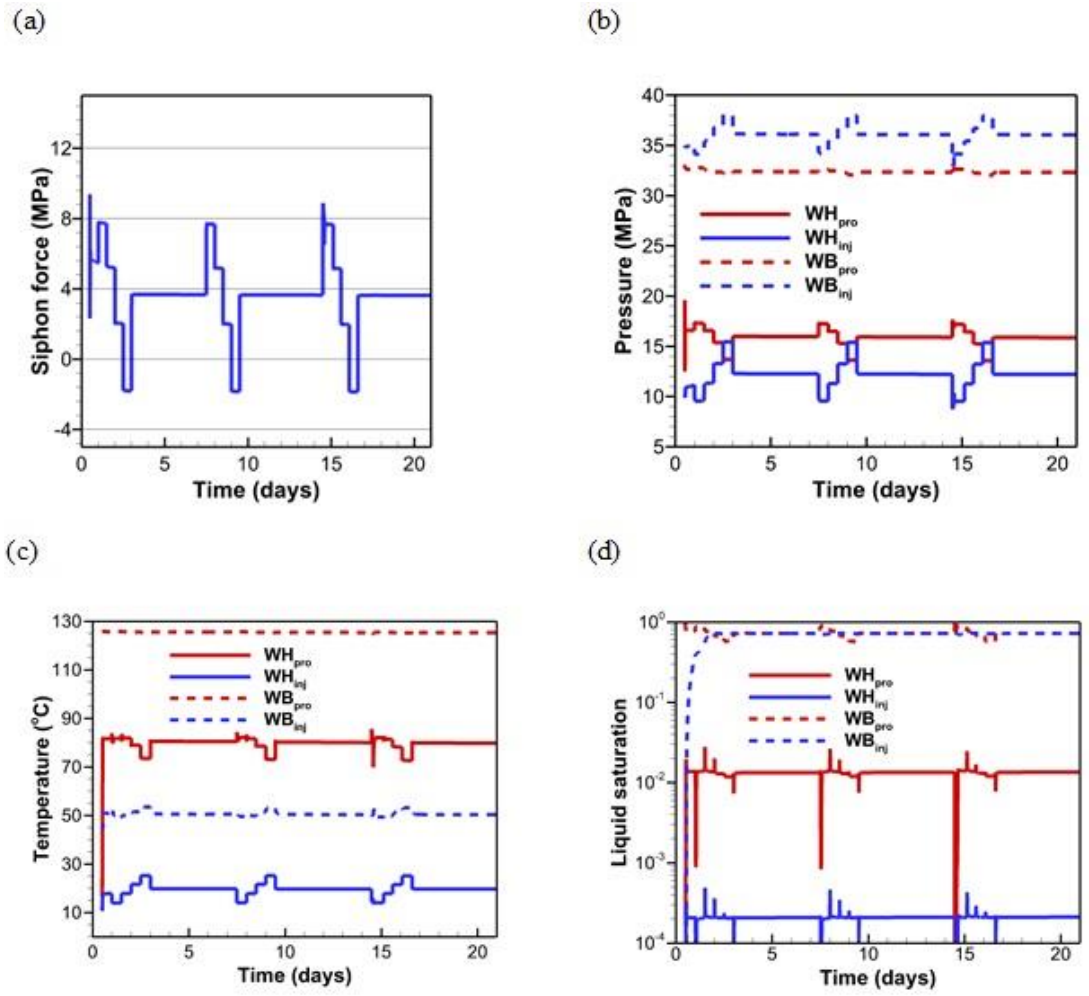

Figure 5. Key results for the Cranfield site model. A thermosiphon can be sustained for flow rates of 2, 4, and 6 kg/s, but not for 8 kg/s.

3. CO_2 THERMOSIPHON FIELD TEST, JANUARY 2015

3.1 FIELD ACTIVITIES

3.1.1 Well Preparation

The Cranfield Thermosiphon test utilized well F3 as a producer and well F1 as an injector operated as a two-well dipole. Data required to calibrate our flow model includes well-head pressure and temperature, bottom-hole pressure and temperature, recirculation rate and fluid density. The upsteam and downstream pressure and temperature across the heat exchangers were also recorded so as to provide an estimate for the heat extracted by the chiller. We also installed a distributed temperature sensor (DTS) to record the temperature of the flowing fluid column in the F3 producer.

The F3 well was completed with a tubing and packer prior to the initiation of our field trial. In order to record bottomhole pressure and DTS temperature, we hung a hybrid fiber-optic /copper control line in the well to operate simultaneously a quartz pressure sensor (Ranger Gauge Systems, Rosharon, TX, USA) and record DTS profiles. Figure 6a shows the installation of the hybrid control line using a capillary head injector. The capillary unit acts as a miniature coiled-tubing rig as it has rollers that can both feed and remove the ¼" capillary line from the well. Figure 6b is the F3 well as completed with a short lubricator and pack-off at the wellhead for pressure control. The quartz gauge records pressure with an accuracy of 0.015% of the full-scale range of the gauge, as well as temperature, which can be used for calibrating the DTS profiles.

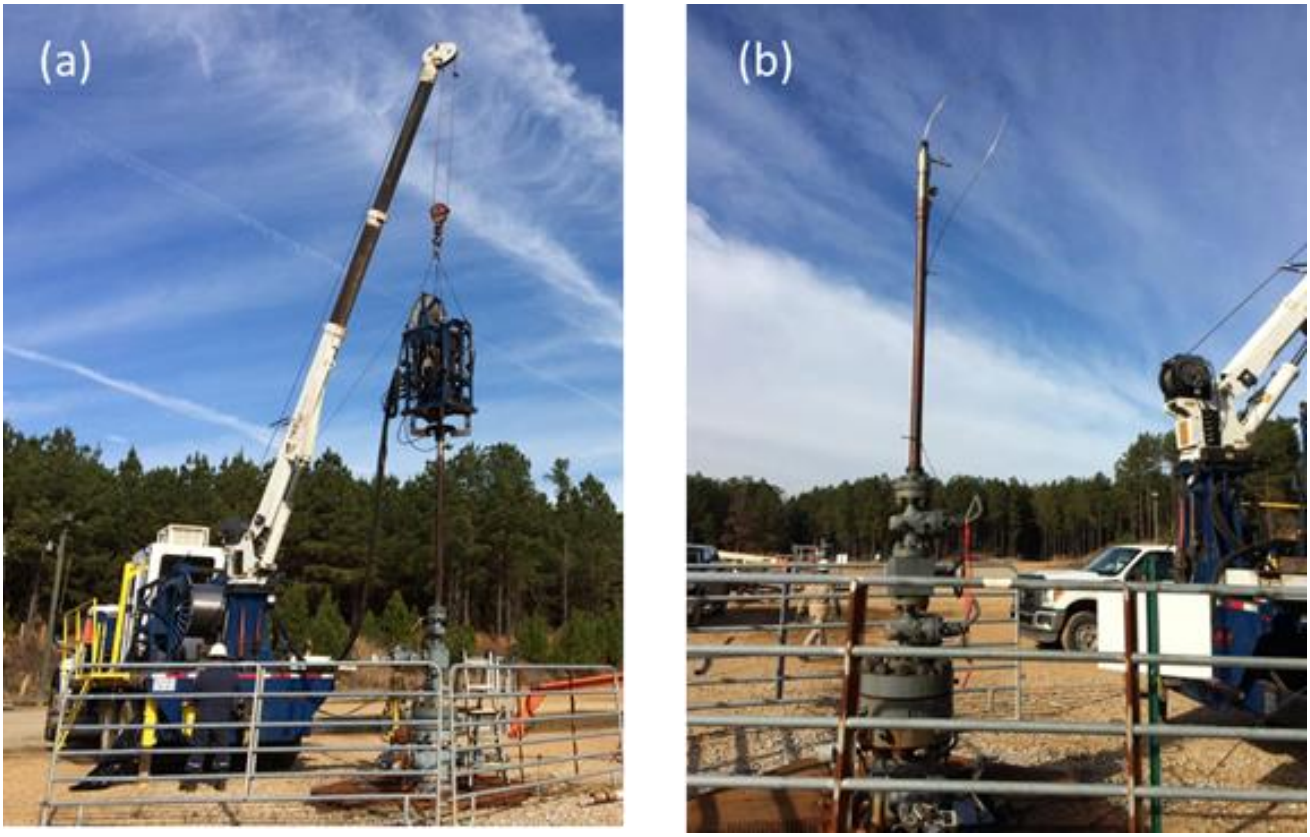

Figure 6. Installation of a hybrid fiber-optic/copper control line in the F3 well for simultaneous monitoring of bottomhole pressure and collecting DTS profiles.

3.1.2 Thermosiphon Monitoring and Control Equipment

A schematic layout for the surface equipment used during the thermosiphon test is shown in Figure 7. All of the surface equipment was installed and commissioned in the first three days in the field, from January 19 – 21, 2015. The equipment on the schematic in blue is the chilling equipment that was leased from Carrier Rentals. The Emerson Micromotion flowmeter was specified to be able to measure with high accuracy the density of the fluid stream, so that we could estimate the brine-to-CO_2 ratio. The automated valving was installed with the objective of operating in an unattended mode with computer supervision. Before and after each critical control point, the pressure and temperature of the flowing fluid were monitored. Figure 8 shows the set-up of the instrumentation, which on the schematic is in the green highlighted area of Figure 7, labeled "Equipment at F3." Figure 9 shows the flow iron running between F3 and F1 for the recirculation of the CO_2.

One of the critical components in performing the thermosiphon test program was to have a way to remove heat from the CO_2 before it was reinjected into the F1 well. To accomplish this we leased from Carrier Rentals a 100 T chiller, which was installed near the F1 injection well. This was used to circulate chilled glycol and water through high-pressure Heatric heat-exchangers (Heatric, Poole, UK). The Heatric exchangers consist of diffusion bonded printed steel plate microchannels, occupying only ¼ of the volume of conventional tube heat exchangers. Figure 10 shows the heat exchangers with the 100T chiller and surge tank in the background. On the left side of the image is the painted red F1 injection well. The blue stand on the right side of the picture is holding the two Heatric heat exchangers, used in series to increase heat exchange capacity.

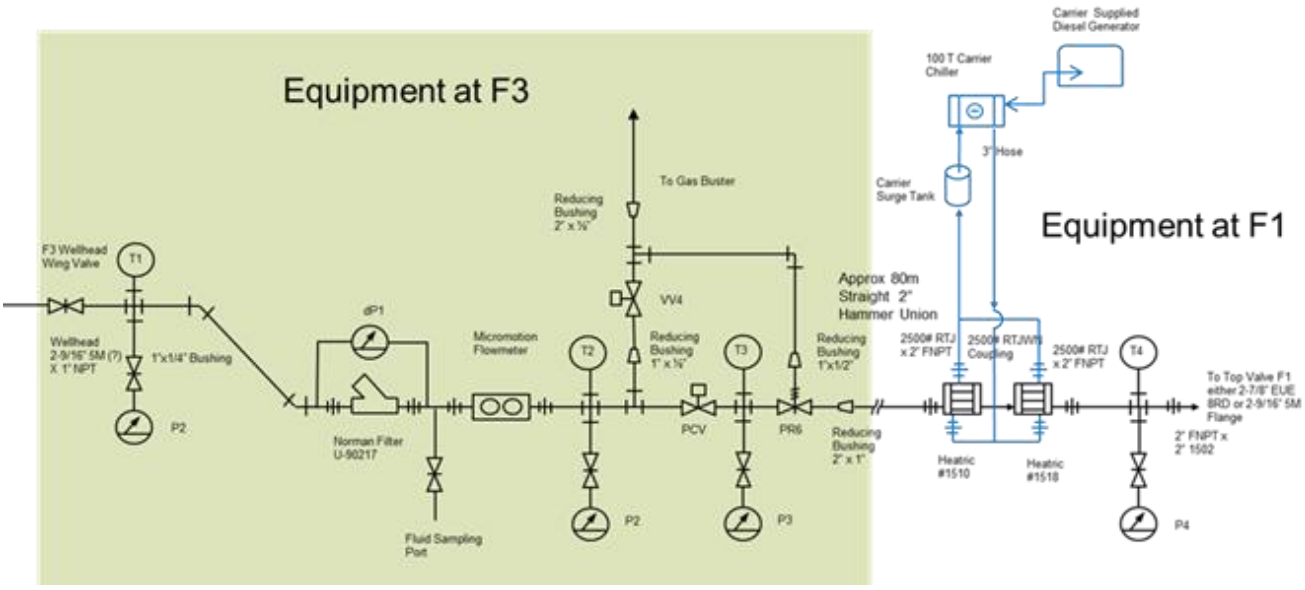

Figure 7. Schematic of the equipment used for conducting the Cranfield thermosiphon test.

Figure 8. F3 production well with computer actuated valve system and Emerson Micromotion Coriolis mass flowmeter to control and monitor the CO_2 production. F3 wellhead can be seen in the background.

Figure 9. Flow iron looking toward F1 well from F3 well. This is the main recirculation loop for geothermally heated CO_2. The F2 welllhead appears in the foreground with the more distant F1 wellhead painted red beyond it.

Figure 10. Two Heatric heat exchangers are located on the blue stand, with a 100 T chiller and surge tank in the background.

3.1.3 Thermosiphon Operation

In order to kick-off the thermosiphon, that is, to increase the wellhead pressure at F3 such that CO_2 would naturally flow between the F3 production well and the F1 injection well, we added a vent valve and directed the CO_2 into a "gas buster" frac tank. On the schematic

drawing (Figure 7) the vent valve is shown as VV4. When the vent valve is opened, hot CO_2 rapidly moves up the F3 production well; with hotter, less dense fluid in the well, F3 wellhead pressure increases. During venting, the flow line to the F1 injection well is closed, so its pressure does not change. Figure 11 shows the frac tank being used to vent the CO_2. When venting is ongoing a safety protocol is followed with all personnel kept up-wind of the venting gas and gas levels on the well pad continuously monitored. After venting ends, all flow lines are opened and thermosiphon flow from F3 to F1 commences.

Figure 11. Venting operations from the F3 well into a "gas buster" equipped frac tank. The tank is designed to allow for dispersion of gas and collection of liquids during well venting operations.

There were three venting operations followed by recirculation (thermosiphon) between F3 and F1, accompanied by collection of data. The first venting operation used the schematic shown in Figure 7. Subsequent venting operations bypassed the Coriolis flowmeter, in order to maximize the flowrate, so for these venting events, we can only estimate the flowrate by analyzing the drawdown. Figure 12 shows a schedule of events, along with the mass flow rate through the system. During all siphon periods, flow rate steadily declines, indicating that a thermosiphon is not sustained.

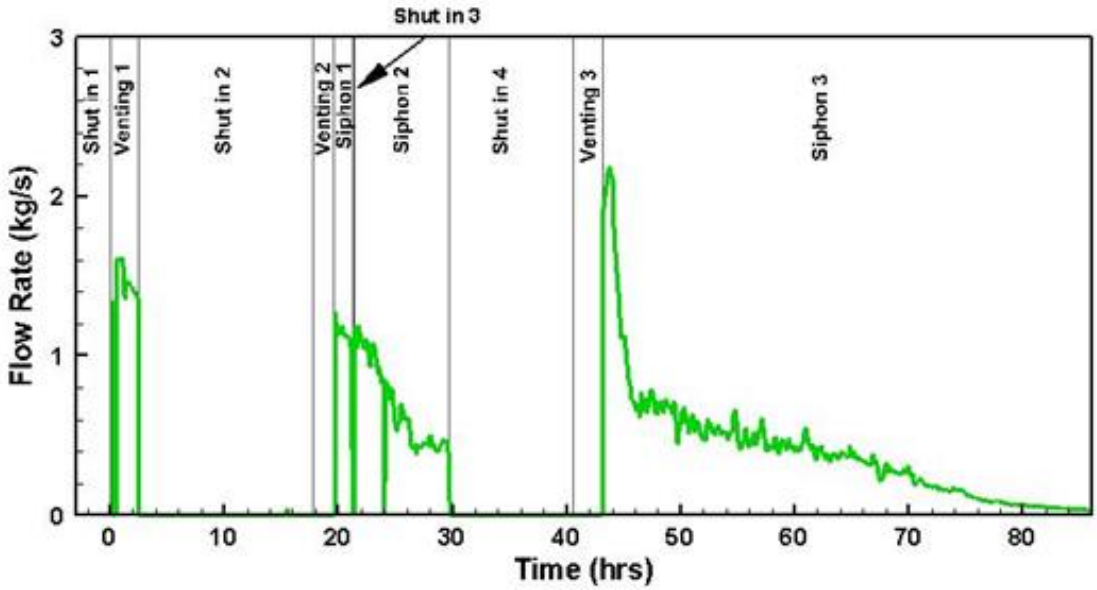

Figure 12. Sequence of events during 4 days of thermosiphon testing, along with the flow rate through the system.

3.2 Data Collected

Data collection included the following parameters:

- DTS fiber-optic temperature logs of F2 and F3 well
- Quartz pressure and temperature from the reservoir interval in F2 and F3
- Fluid pressure and temperature at the outlet of the F3 production tubing
- Differential pressure across the 100 μ filter unit
- Emerson Micromotion Coriolis measurement of the fluid mass flux rate and density
- Pressure and temperature at the Coriolis flowmeter exit
- Pressure and temperature downstream of the recirculation pressure control valve
- Pressure and temperature at the outlet of the heat exchangers and inlet to F1

Figures 13 and 14 show key surface measurements during the longest of the three recirculation periods. In Figure 13, the near-constant F1 temperature reflects the outlet of the chiller. The driving force for the thermosiphon is the difference in wellhead pressures between F3 and F1, which is seen to steadily decrease with time. The F3 production temperature declines in concert with the pressures. Figure 14 shows the flow rate and density of the recirculating fluid, measured at the Coriolis flow meter. The flow rate shows some small short-term variability, but generally declines with the same trend as the surface pressures. Fluid density shows sharp oscillations, which represent slugs of liquid water being produced along with the supercritical CO_2. If we assume that the values at the bottom of the density envelope represent pure CO_2 and the values at the top of the density envelope represent pure water, then the average density reflects the average water mass fraction in the produced fluid, which is about 0.18.

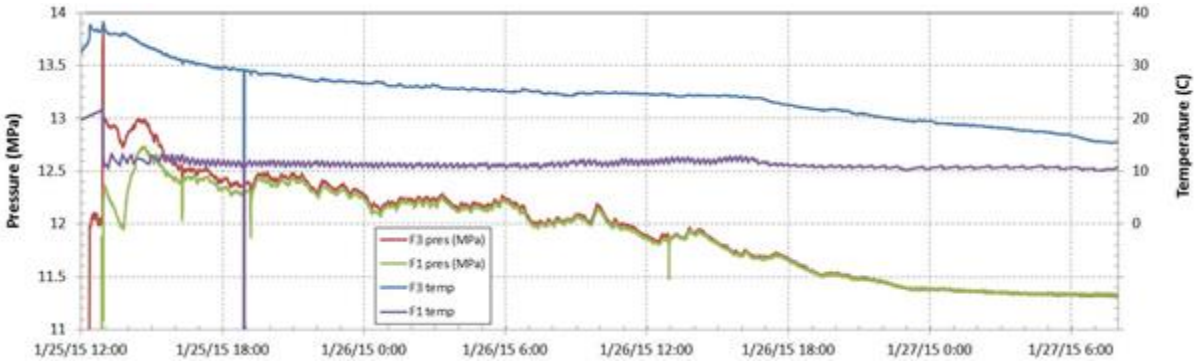

Figure 13. Surface pressures and temperatures at production well F3 and injection well F1 during the final thermosiphon period.

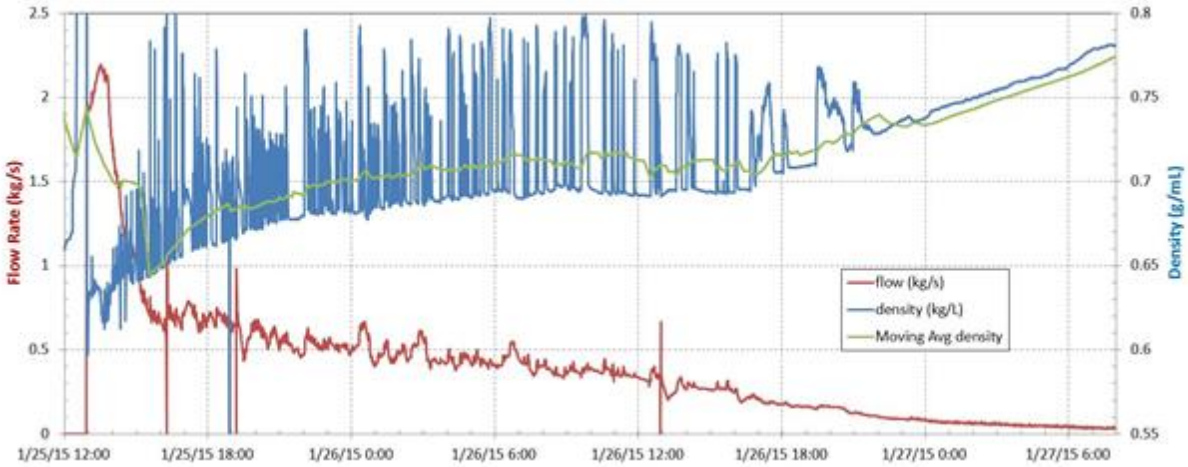

Figure 14. Flow rate and fluid density during the final (and longest) thermosiphon period. The time-averaged density is also shown.

4. MODELING OF THERMOSIPHON FIELD TEST

The model used to analyze the field data is quite similar to the model described in Section 2.2 above, but the following changes were made to include more realism in representation of the field conditions and operations.

- Add heat loss from surface piping.
- Use a more accurate initial vertical temperature profile with a lower surface temperature.
- Represent the shut in, venting, thermosiphon sequence shown in Figure 12.
- Add model layers below the reservoir to enable accurate placement of downhole P,T gauges below the reservoir.
- Do not set the flow rate anywhere in the CO_2 flow path during recirculation. That is, no boundary conditions are set for the CO_2 flow path through the wells, reservoir, or surface piping, nor are any sources or sinks specified. This is quite unusual for a numerical simulation involving injection and production wells, and differs markedly from the previous two models in which mass injection and production rates were specified.

The initial conditions attempt to accurately represent the pre-kick-off conditions. Venting is modeled by introducing a constant-pressure, constant-temperature cell to represent the atmosphere, and connecting it to the surface pipe through a cell that has a choke to control flow rate. The first venting operation, in which flow rate was monitored, was used to calibrate the strength of the choke, and this same calibration was used for the subsequent venting operations also. No other model calibration was done.

Figure 15 shows the surface pressures and temperatures at wells F1 and F3. Both the pressure and temperature differences between production well F3 and injection well F1 remain large and constant, indicating that the driving force for the thermosiphon is not decreasing. Figure 16 shows the modeled flow rate through the system. Flow rate during each recirculation period is steady at about 2 kg/s, confirming that a thermosiphon can be sustained. Most of the fluid is gas, but there is a small liquid mass fraction, about 0.04.

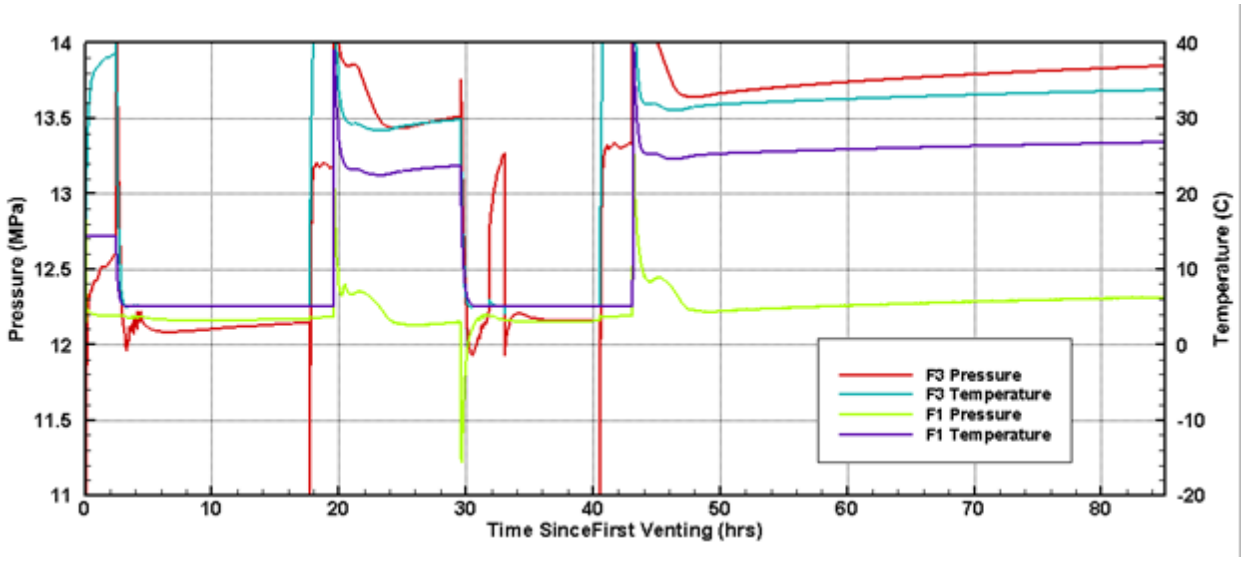

Figure 15. Modeled surface pressures and temperatures at the wells. The first venting period begins at t = 0, and venting lasts about two hours. Subsequent venting operations begin at 18 and 40 hours. Recirculation occurs after the second and third venting operations.

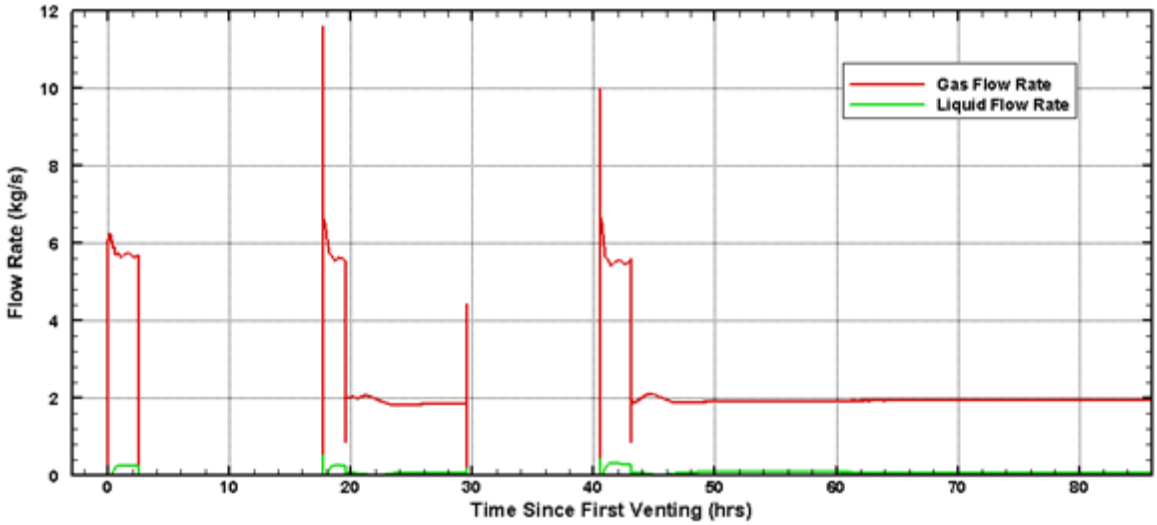

Figure 16. Modeled thermosiphon flow rates. The first venting period begins at t = 0, and venting lasts about two hours. Subsequent venting operations begin at 18 and 40 hours. Recirculation occurs after the second and third venting operations.

5. DIFFERENCES BETWEEN PREDICTIONS AND REALITY

The key difference between the model and field conditions is that the models all predict a sustaining thermosiphon, but in the field we see a thermosiphon that decays rapidly with time. Another difference is that the model shows very little water produced (about 4%), but in the field there is sporadic water production along with the produced CO_2, with average water fraction estimated to be about 18%.

It is worth noting that despite calibration attempts, the flow rate during the first venting operation could not be matched closely while maintaining reasonable model pressures. Additionally, the modeled temperature of the chiller outlet (temperature at well F1) is too large. These will be areas for further model calibration.

6. HYPOTHESES TO ACCOUNT FOR DIFFERENCES BETWEEN PREDICTIONS AND REALITY

It may be that simple model calibrations to better represent surface components, such as those described in the previous paragraph, will be sufficient to enable the model to reproduce the field observations. However, we suspect that more serious changes to the well and reservoir components of the system will be needed also. Below are the features that we believe may be important for determining whether a thermosiphon is sustained or decays.

6.1 Well-related factors

Liquid water in the production well could be damping the thermosiphon. This is justified from first principles in that a geothermal heat extraction system using water as the working fluid would not be expected to sustain a thermosiphon, so inclusion of water in the fluid stream should tend to dampen the thermosiphon. A sensitivity of thermosiphon flow rate to water content is also supported by the sensitivity studies described in Section 2.2. There are two mechanisms by which liquid water could enter the production well:

(1) Liquid water could be mobile in the reservoir. This would require a modification of our conceptual model of the multiphase behavior of supercritical CO_2 and liquid water, which would leave more mobile water in place, even after years of CO_2 injection. This could be accomplished using different relative permeability functions. Another possibility would be to represent the reservoir as a dual permeability medium, in which high-permeability sands are saturated with CO_2 but low-permeability shales remain water-saturated, and this water remains available to move into the production well. The hysteretic behavior of CO_2/brine systems (Doughty, 2007) could complicate this effect.

(2) Liquid water could be immobile in the reservoir, but water that is dissolved in the $scCO_2$ phase at reservoir conditions could condense into a separate aqueous phase as it moves up the wellbore. This effect is not well represented in our current equation of state module for the TOUGH simulator, but can be examined with a new module, ECO2N V2.0 (Pan et al., 2015c). However, the amount of water that can dissolve in the $scCO_2$ phase is small, about 1.7% by mass at reservoir conditions and about 0.1% at wellhead conditions, so it is unlikely to contribute significantly to thermosiphon dampening.

Effective thermal conductivity of the near well-bore region could be higher than the actual thermal conductivity as it includes other physical processes. Sensitivity studies in Section 2.1 indicated that heat transfer from the wellbore to the overburden is very important.

A skin could be needed for the production well. This is plausible because modeling of Cranfield long-term CO_2 injection required a skin around the injection well, and they were drilled using similar procedures. A skin around the production well would increase the pressure drop accompanying flow from the reservoir into the well, so would weaken the thermosiphon.

The friction factors for the wells may be too small. A larger friction factor would require a greater pressure drop in the well, which would weaken the thermosiphon.

6.2 Reservoir-related factors

The intrinsic permeability distribution in the reservoir could include a fast path between injection and production wells, short-circuiting the thermal heat exchange with reservoir rock. Previous simulations of the GCS operation at Cranfield (Doetsch et al., 2013) required some preferential flow, but probably not enough to be considered a short circuit. A dual permeability model would also be a good way to represent the high permeability sands and low permeability shales, which respond very differently to pressure and temperature gradients.

The far-field boundary conditions, representing operations of a CO_2-flood EOR operation, could be incorrect. We have seen in previous studies that thermosiphon behavior is sensitive to the background pressure of the system.

7. CONCLUSIONS

Detailed pre-test modeling showed that a sustained thermosiphon should be possible at the Cranfield site. However, in the field we were able to initiate a thermosiphon, but it decayed over time. We have several hypotheses to explain this discrepancy including the production of water above predictions tending to work against the thermosiphon as well as higher than estimated effective thermal conductivity of the well. We will test our hypothesis in future work. These findings may point to a fundamental limitation in the ability to sustain a CO_2 thermosiphon or lead to a modification in how we need to consider operating a thermosiphoning system.

ACKNOWLEDGEMENTS

We would like to thank Sue Hovorka, Alex Sun and Jiamin Lu , Gulf Coast Carbon Center, Texas Bureau of Economic Geology for their help in supporting our field work. This work was funded by the Assistant Secretary for Energy Efficiency and Renewable Energy, Geothermal Technologies Program of the U.S. Department of Energy through contract to Lawrence Berkeley National Laboratory under Contract No. DE-AC02-05CH11231.

REFERENCES

Brown, D. A hot dry rock geothermal energy concept utilizing supercritical CO2 instead of water. In: Proceedings of the Twenty-fifth Workshop on Geothermal Reservoir Engineering, Stanford University, CA, USA, pp. 233–238, 2000.

Doetsch, J., M.B. Kowalsky, C. Doughty, S. Finsterle, J.B. Ajo-Franklin, C.R. Carrigan, X. Yang, S.D. Hovorka, and T.M. Daley, Constraining CO2 simulations by coupled modeling and inversion of electrical resistance and gas composition data, *International Journal of Greenhouse Gas Control*, 18, 510-522, 2013.

Doughty, C., Modeling geologic storage of carbon dioxide: comparison of hysteretic and non-hysteretic curves, *Energy Conversion and Management*, 48, 6, 1768-1781, 2007.

Doughty, C. and B.M. Freifeld. Modeling CO2 injection at Cranfield, Mississippi: Investigation of methane and temperature effects, *Greenhouse Gas Sci Technol*. 3, 475–490, 2013.

Hosseini, S.A., H. Lashgari, J.W. Choi, J.-P. Nicot, J. Lu, and S.D. Hovorka, Static and dynamic reservoir modeling for geological CO2 seuestration at Cranfield, Mississippi, U.S.A., *International Journal of Greenhouse Gas Control*, 18, 449-462, 2013.

Pan L., S.W. Webb, and C.M. Oldenburg. Analytical solution for two-phase flow in a wellbore using the drift-flux model. *Advances in Water Resources*, 34, 1656–1665, 2011a.

Pan L., C.M. Oldenburg, K. Pruess, and Y.-S. Wu. Transient CO2 leakage and injection in wellbore-reservoir systems for geologic carbon sequestration. *Greenhouse Gas Sci Technol*, 1, 335–350, 2011b.

Pan, L., Y.-S. Wu, C.M. Oldenburg, and K. Pruess. T2Well/ECO2N Version 1.0: Multiphase and Non-Isothermal Model for Coupled Wellbore-Reservoir Flow of Carbon Dioxide and Variable Salinity Water. LBNL-4291E, 2011c.

Pan, L., and C. M. Oldenburg. T2Well—An integrated wellbore-reservoir simulator. *Computers & Geosciences* 65 (2014) 46–55, 2013.

Pan, L., C. Doughty, B. Freifeld, and C.M. Oldenburg, Modeling a CO2 thermosiphon in a partially saturated reservoir using W2Well with EOS7CMA, in Proceedings, TOUGH Symposium 2015, Lawrence Berkeley National Laboratory, Berkeley, California, September 28-30, 2015a.

Pan, L., B. Freifeld, C. Doughty, S. Zakem, M. Sheu,B. Cutright, T. Terrall, Fully coupled wellbore-reservoir modeling of geothermal heat extraction using CO2 as the working fluid, *Geothermics* 53, 100–113, 2015b.

Pan, L., N. Spycher, C. Doughty, and K. Pruess, ECO2N V2.0: A TOUGH2 fluid property module for mixtures of water, NaCl, and CO2, Rep. LBNL-6930E, Lawrence Berkeley National Lab., Berkeley, CA, February 2015c.

Pruess, K. Enhanced geothermal systems (EGS) using CO2 as working fluids – a novel approach for generating renewable energy with simultaneous sequestration of carbon. *Geothermics*, 35, 351-367, 2006.

Pruess, K., C.M. Oldenburg, and G.J. Moridis. TOUGH2 User's Guide Version 2. Lawrence Berkeley National Laboratory Report, LBNL-43134, November 1999.

Pruess, K., and N. Spycher. ECO2N – a fluid property module for the TOUGH2 code for studies of CO2 storage in saline aquifers. *Energy Conversion and Management*, 48, 1761-1767, 2007.